CO_2-system development in young sea ice and CO_2 gas exchange at the ice/air interface mediated by brine and frost flowers in Kongsfjorden, Spitsbergen

Agneta FRANSSON,[1,2] Melissa CHIERICI,[3,4] Katarina ABRAHAMSSON,[3] Maria ANDERSSON,[3]* Anna GRANFORS,[3] Katarina GÅRDFELDT,[5] Anders TORSTENSSON,[6] Angela WULFF[6]

[1]*Norwegian Polar Institute, Fram Centre, Tromsø, Norway*
E-mail: agneta.fransson@npolar.no
[2]*Department of Earth Sciences, University of Gothenburg, Göteborg, Sweden*
[3]*Department of Chemistry and Molecular Biology, University of Gothenburg, Göteborg, Sweden*
[4]*Institute for Marine Research, Tromsø, Norway*
[5]*Centre for Environment and Sustainability, Chalmers University of Technology, University of Gothenburg, Göteborg, Sweden*
[6]*Department of Biological and Environmental Sciences, University of Gothenburg, Göteborg, Sweden*

ABSTRACT. In March and April 2010, we investigated the development of young landfast sea ice in Kongsfjorden, Spitsbergen, Svalbard. We sampled the vertical column, including sea ice, brine, frost flowers and sea water, to determine the CO_2 system, nutrients, salinity and bacterial and ice algae production during a 13 day interval of ice growth. Apart from the changes due to salinity and brine rejection, the sea-ice concentrations of total inorganic carbon (C_T), total alkalinity (A_T), CO_2 and carbonate ions (CO_3^{2-}) in melted ice were influenced by dissolution of calcium carbonate ($CaCO_3$) precipitates (25–55 µmol kg^{-1}) and played the largest role in the changes to the CO_2 system. The C_T values were also influenced by CO_2 gas flux, bacterial carbon production and primary production, which had a small impact on the C_T. The only exception was the uppermost ice layer. In the top 0.05 m of the ice, there was a CO_2 loss of ~20 µmol kg^{-1} melted ice (1 mmol m^{-2}) from the ice to the atmosphere. Frost flowers on newly formed sea ice were important in promoting ice–air CO_2 gas flux, causing a CO_2 loss to the atmosphere of 140–800 µmol kg^{-1} d^{-1} melted frost flowers (7–40 mmol m^{-2} d^{-1}).

KEYWORDS: atmosphere/ice/ocean interactions, ice chemistry, polar and subpolar oceans, sea-ice dynamics

INTRODUCTION

Changes in the Arctic Earth System (e.g. decreased ice extent and thickness) have been reported, and in September 2012 the lowest ice extent on record was observed (Parkinson and Comiso, 2013). As sea-ice extent decreases and freshwater volume increases, the biogeochemical processes will change. As a consequence, the marine environment, vertical carbon transport and carbon dioxide (CO_2) exchange between the atmosphere and ocean will all be altered.

Processes in the sea ice affect the CO_2 system (or carbonate system) within the sea ice and at the interfaces with the air and the underlying water (e.g. DeLille and others, 2007; Rysgaard and others, 2007; Nomura and others, 2009; Fransson and others, 2011, 2013; Miller and others, 2011a,b). Brine rejection transporting chemical substances between the atmosphere and water is important for CO_2 transport from the atmosphere to deeper layers of water (e.g. Rysgaard and others, 2007; Else and others, 2011). Brine is transported within the sea ice. It is transported downwards due to gravity and upwards at ice formation due to a freezing ice layer near the bottom. This reduces the permeable channels and hence squeezes brines upward. Frost flowers are sometimes formed in this process, as the brine produces a brine skim on the ice surface (Perovich and Richter-Menge, 1994; Alvarez-Aviles and others, 2008). Frost flowers are crystalline structures that form on new sea ice when the air, which is supersaturated with water vapour, condenses at the ice surface. They carry high concentrations of chemical substances, gases, bacteria and salts (e.g. Deming, 2010; Douglas and others, 2012; Fransson and others, 2013; Geilfus and others, 2013; Granfors and others, 2013) and have a 40% larger surface area than sea ice (Domine and others, 2005), promoting gas exchange with the atmosphere. Frost flowers are easily destroyed by wind or blowing snow and consequently only have a brief life span of a few days (e.g. Deming, 2010).

The importance of sea ice for the CO_2 system characteristics in the underlying water has been shown by Fransson and others (2013). Changes in the underlying water will occur during the sea-ice season. This is due to the increased CO_2 in brine and depletion in A_T compared to C_T due to $CaCO_3$ precipitation during ice freezing (Rysgaard and others, 2007, 2013; Fransson and others, 2011, 2013) and the excess A_T in relation to C_T and salinity during ice melt. Solid $CaCO_3$ in the form of ikaite has previously been found in Arctic sea ice (Dieckmann and others, 2010; Rysgaard and others, 2012, 2013; Nomura and others, 2013). When

*Present address: Volvo Cars Cooperation, Göteborg, Sweden.

https://doi.org/10.3189/2015AoG69A563 Published online by Cambridge University Press

Table 1. Sampling dates of young landfast sea ice, brine and under-ice water, ice thickness of young ice, and meteorological data (mean air temperature, mean wind speed and mean relative humidity) from Ny-Ålesund weather station (8 m a.s.l.) at the study site in Thiisbukta (78.927° N, 11.901° E), and date for sampling thicker landfast sea ice at Engelskbukta (EB; 78.832° N, 11.895° E). EB is located on the other side of the Brøgger Peninsula 10 km from Ny-Ålesund (flight distance). See Figure 1 for map location. Note that under-ice water (0–2 m) was collected parallel to sea-ice sampling. There was no snow cover at the site and no precipitation during the study

Date (2010)	Study day	Sky	Young-ice thickness	Air temp.	Wind speed	Relative humidity
			m	°C	m s^{-1}	%
21 Mar	0	Fair	0.27	–9.7	5.6	60
22 Mar	1	Sunny	0.27	–12.4	3.7	53
23 Mar	2	Sunny	0.28	–14.5	1.2	56
24 Mar	3	Cloudy	0.31	–13.7	1	64
26 Mar	5	Fair	0.33	–15.6	0.9	73
27 Mar	6	Sunny	0.34	–15.9	1.6	62
28 Mar	EB	Fair	0.42	–12.8	2.3	61
29 Mar	8	Fair	0.36	–14.1	1.5	56
30 Mar	9	Sunny	0.37	–14.3	7.2	54
31 Mar	10	Fair	0.38	–8.8	6.1	60
1 Apr	11	Fair/cloudy	0.41	–10.3	1.9	54
2 Apr	12	Fair/cloudy	0.38	–10.7	1.4	50

solid $CaCO_3$ precipitates in the sea ice, CO_2 is released to the aqueous phase, and when it dissolves, CO_2 is consumed:

$$Ca^{2+} + 2HCO_3^- \Leftrightarrow CaCO_3(s) + H_2O + CO_2(aq) \quad (1)$$

The solid $CaCO_3$ may be left in the ice until the onset of melt, during melt or when the ice becomes porous enough to release the $CaCO_3$ to the underlying water (e.g. Lyakhin, 1970). This (intermittent) storage changes the ratios between the CO_2 system parameters and salinity, and changes the vertical carbon fluxes and ice–air CO_2 gas flux (e.g. Fransson and others, 2013). Ice–air CO_2 gas fluxes were previously estimated in Arctic sea ice and showed that CO_2 escaped from the ice to the atmosphere during sea-ice formation (Papadimitriou and others, 2004; Nomura and others, 2006; Else and others, 2011, 2012; Miller and others, 2011a,b; Papakyriakou and Miller, 2011; Rysgaard and others, 2012; Fransson and others, 2013).

It has been demonstrated that biological processes (e.g. primary production and bacterial respiration) are responsible for the variability of the sea-ice CO_2 system (e.g. Fransson and others, 2011, 2013). In winter, bacterial respiration is an important process for the production of CO_2 at the bottom of the ice, causing an increase in C_T and CO_2 gas flux from the ice (Fransson and others, 2013). In spring, primary production in the bottom ice consumes CO_2, causing a decrease in C_T, which results in CO_2 uptake by the ice from the surrounding environment (Fransson and others, 2013).

In this study, we investigate the development of the CO_2 system in young sea ice, focusing on the effect of sea-ice processes in the role of CO_2 exchange at the ice/air interface during a 13 day interval in Kongsfjorden, West Spitsbergen, Svalbard. To our knowledge, this is the first CO_2 system study performed in a fjord of Spitsbergen. We present: (1) the evolution of the CO_2 system of young sea ice; (2) an estimate of the effect of the biogeochemical processes (e.g. bacterial and primary production and $CaCO_3$ precipitation/dissolution); (3) estimates of CO_2 gas fluxes at the ice/air interface; and (4) a discussion of the importance of frost flowers for CO_2 transport from the ice to the atmosphere.

STUDY AREA

The ice study was carried out between 21 March and 2 April 2010, in the Thiisbukta Bay area in Kongsfjorden, ~500 m from Ny-Ålesund, West Spitsbergen, at 78.927° N, 11.901° E (Fig. 1). The total surface area of the bay is ~10 000 m^2 (Fig. 2a). The thickness of the young landfast sea ice (referred to as young ice) was 0.27 m at the start of the study and was formed by freezing of pancake ice (Fig. 2a). Throughout the study, the young ice was void of snow, but frost flowers occasionally formed near the study area (Fig. 2b). On a few occasions, we sampled thin pancake ice (PCI; newly formed sea ice, 0.04 m) near Thiisbukta (TB). In addition to TB sea ice, on 28 March we sampled thicker landfast sea ice (0.42 m thick) in Engelskbukta (EB; 78.832° N, 11.895° E; Fig. 1), situated 10 km (flying distance) from Ny-Ålesund on the other side (southern part) of the Brøgger Peninsula (Fig. 1).

The average daily air temperature varied between –9°C and –16°C. The lowest temperature was recorded on 27 March and the highest on 31 March (Table 1). The average daily wind speed varied between 1 and 6 m s^{-1}. The highest wind speed was recorded on 31 March (data courtesy of Norwegian Meteorological Institute). The measuring site is located 8 m a.s.l. and 570 m from the TB study area. The light conditions, obtained from our own measurements of photosynthetically active radiation (PAR; 400–700 nm), varied between zero (during all the nights) and the maximum value of 800 µmol photons m^{-2} s^{-1} on 26 March, At the end of the study, due to cloudy conditions this dropped to 350–400 µmol photons m^{-2} s^{-1} (Table 1). In the sea ice, the radiation measurements of incident PAR showed that 8% remained at a depth of 0.35 m (at midday).

METHODS

Sampling of bulk sea ice, brine, frost flowers and underlying water

During the 13 day study, we collected young ice cores for carbonate chemistry on 11 occasions (21, 22, 23, 24, 26, 27, 29, 30 and 31 March and 1 and 2 April 2010; Table 2).

https://doi.org/10.3189/2015AoG69A563 Published online by Cambridge University Press

Fig. 1. Map of the study site at Thiisbukta (78.927° N, 11.901° E) and location of sampling for young landfast sea ice, brine, under-ice water, frost flowers and newly formed pancake ice. Landfast sea ice and brine sampling at Engelskbukta (78.832° N, 11.895° E) is denoted as EB on the map.

Samples of microalgal and heterotrophic bacterial abundances and activities in the young ice were collected on five occasions (21, 23, 26, 29 and 31 March 2010). Additional ice-core sampling of ice in Engelskbukta and pancake thin ice was performed during the study. Sea-ice cores were sampled using a stainless-steel ice-core drill (diameter 0.12 m) with a power head. The ice cores were divided into 0.05 m sections, which were individually placed into Tedlar© gas-sampling bags. After carefully removing surrounding air from the bags using a hand-operated vacuum pump (Nalgene©), the bulk sea-ice samples (hereafter referred to as sea ice) were slowly thawed in darkness for ~24 hours to reach a temperature varying between 4°C and 10°C. No solid calcium carbonate ($CaCO_3$) was observed in our samples. This is likely because on some occasions the sample temperature exceeded 4°C. The resulting volume of the melted sea ice was ~0.5 L. Microbiological abundance and activity were sampled from separate ice cores collected within a 0.2 m radius of the cores sampled for chemical analysis. The ice cores were immediately wrapped in black plastic to protect the algae from light stress, and were cut into 0.05 m sections for further processing at 0°C.

In parallel to ice-core sampling, brine samples were collected (Table 3) in 0.1 L borosilicate glass bottles (airtight) from partially drilled holes (known as sackholes) in young sea ice (hereafter referred to as YI). We refer to these samples as brine. The brine, which had seeped into the sackhole at different depths in the ice (0.1–0.2 m), was collected with a plastic syringe and PVC tubing after ~30–40 min and transferred to the bottles. Due to the cold sea-ice conditions, the volumes of brine were usually insufficient for analysis and studies of the full CO_2 system. Further, we could only collect brine samples on three occasions during the study. The sackholes were covered with a plastic isolated lid to

https://doi.org/10.3189/2015AoG69A563 Published online by Cambridge University Press

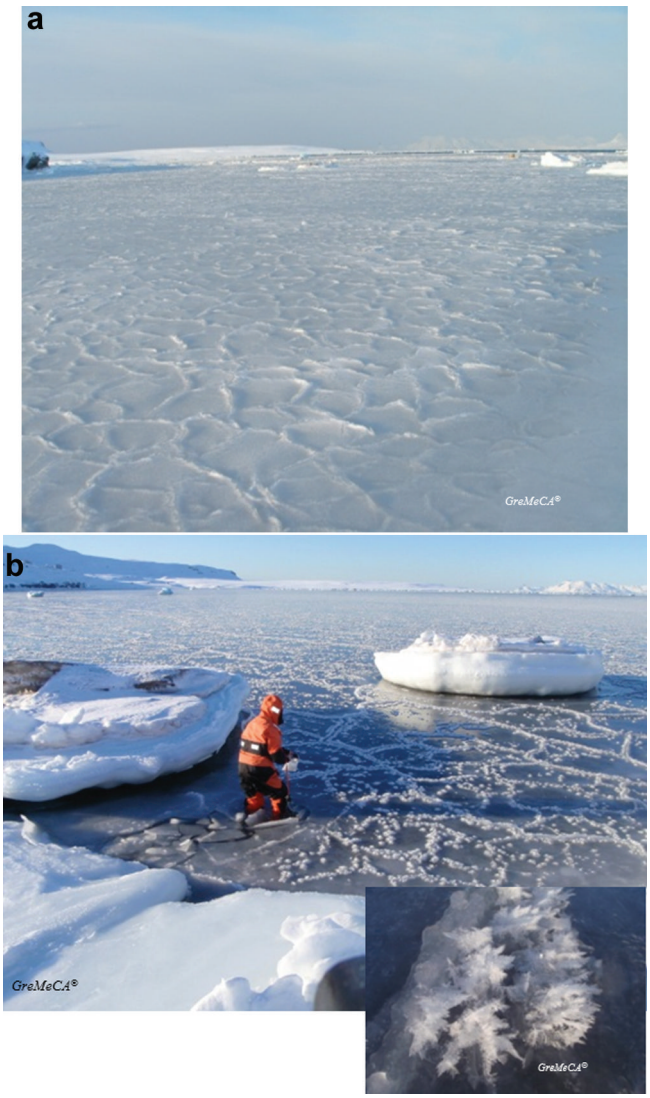

Fig. 2. Photographs showing (a) the Thiisbukta site, and (b) the sampling of newly formed frost flowers (magnified frost flowers picture included).

minimize gas exchange with the atmosphere and prevent freezing of the brine. During our study, the seeping time for brine was sometimes >30 min to allow for sufficient sample volume (0.5–0.1 L). Consequently, the occurrence of some gas exchange cannot be excluded.

Under-ice water (UIW) was collected in 0.25 L borosilicate glass bottles on every occasion when sea-ice cores were sampled, using a glass bottle on a (custom-built) shaft immersed through the borehole. Although debris from the ice was removed before sampling, some debris may be left in the water collected. The water and brine samples were immediately placed in an insulated cooling box to prevent them from freezing.

Frost flowers were sampled ~200 m from our study site on 27 and 28 March using a Teflon ladle from a surface area of 1 m^2 for each sample. The frost flowers were sampled (duplicate) as soon as they formed, and again 20 hours later (one sample). The samples were packed in Tedlar© sampling bags, and the air was gently removed using the hand-operated vacuum pump. After removing the surrounding air from the bags, the samples were thawed in darkness. The melted volume was ~1 L.

Sea-ice temperature was measured on site immediately after the ice core was recovered, at 0.05 m intervals using a digital thermistor (Amadigit) with an accuracy of ±0.1°C. The holes for the temperature measurement were carefully drilled manually with a clean stainless-steel hand drill to avoid additional heating from the drill. The temperature of brine was measured in the sackhole before it was transferred to a sample bottle. UIW temperature was measured in the sample bottle immediately after sampling using the same handheld thermistor probe (Amadigit).

Data and analysis

After melt of the bulk sea-ice and frost flower samples, we measured the CO_2 system parameters, nutrients, bacterial and algal activity and salinity in the melted samples. All sea-ice and frost-flower measurements are hereafter referred to as concentrations and activities in melted samples.

CO_2 system

We measured the CO_2 system (also referred to as the carbonate system) parameters of total alkalinity (A_T) and pH in melted sea ice, brine, frost-flower melt and UIW, using the same method as Fransson and others (2011). A_T and pH in sea ice and frost flowers referred to in this study were always measured in liquid phase (sea ice and frost-flower melt). A_T was determined by potentiometric titration in an open cell (Dickson and others, 2007) with A_T measurement precision of ±3 μmol kg^{-1}. The pH was determined spectrophotometrically using a 2 mM solution of the sulphonaphtalein dye *m*-cresol purple (Sigma-Aldrich®), as an indicator valid for water $30 > S > 37$ (Clayton and Byrne, 1993). The accuracy of the pH measurements is determined by the accuracy of the determination of the equilibrium constants of the dye, which is ~±0.002 (Dickson, 1993). We used the same indicator batch for the whole study, and studied pH changes between days, so the systematic error due to indicator impurities (Yao and others, 2007) would induce the same error for all measurements. For cold-ice brines, the salinity usually exceeds 40, reducing the accuracy of the measurements. However, Hare and others (2013) investigated the deviation regarding high salinities and low temperatures using *m*-cresol purple, and found that the natural variability in sea ice and brine is larger than the analytical uncertainty. The samples were thermostatted to 15°C prior to analysis. Samples were measured in a 0.01 m cell. The analytical precision was estimated to ±0.001 pH units, which was determined by a series of ten analyses of a sample. The pH of the indicator solution was measured daily using a 0.0002 m cell. The precision was checked by triplicate analysis of one sample every second day. The perturbation of sea-water pH caused by the addition of the indicator solution was calculated and corrected for using the method described by Chierici and others (1999).

The A_T and pH values, measured at 15°C (pH_{15}), salinity and temperature along with the CO_2 calculation program CO2SYS (Pierrot and others, 2006) were used to calculate total inorganic carbon (C_T (μmol kg^{-1}), sometimes referred to as DIC or TIC), carbonate ion concentration ($[CO_3^{2-}]$), CO_2 concentrations ($[CO_2]$; μmol kg^{-1}), partial pressure of CO_2 (pCO_2) and fugacity of CO_2 (fCO_2). All calculated CO_2 system parameters mentioned in this study are derived from A_T and pH measured in liquid (melted) phase. The CO_2 system dissociation constants (K1 and K2) estimated by Roy and others (1993, 1994) were used, since an internal

https://doi.org/10.3189/2015AoG69A563 Published online by Cambridge University Press

Table 2. Physical and carbonate system properties of young landfast sea ice in Thiisbukta

Date		S	Ice T °C	A_T µmol kg^{-1}	C_T µmol kg^{-1}	fCO_2 µatm	$[CO_3^{2-}]$ µmol kg^{-1}	$[CO_2]$ µmol kg^{-1}	$A_T:C_T$	$A_T:S$	$C_T:S$
21 Mar	median	8.5	–5.6	529	504	47	17	4	1.05	64	61
	min	8.0	–6.7	447	427	42	12	4	1.05	63	58
	max	13.2	–3.1	816	757	54	36	5	1.08	65	62
22 Mar	median	9.3	–4.8	592	560	46	22	4	1.06	64	61
	min	8.2	–6.0	546	517	23	19	2	1.06	62	53
	max	14.7	–3.2	916	785	59	78	5	1.17	72	68
23 Mar	median	8.4	–7.6	561	528	34	20	4	1.06	65	63
	min	7.9	–9.9	517	495	33	15	3	1.04	64	60
	max	11.5	–3.8	741	686	49	33	4	1.08	67	63
24 Mar	median	9	–6.7	592	560	43	20	4	1.06	66	62
	min	8.5	–9.2	566	534	33	18	4	1.06	64	59
	max	12.3	–3	791	725	59	39	5	1.09	67	63
26 Mar	median	8.6	–7.1	580	555	43	17	4	1.04	66	66
	min	7.8	–9.5	514	490	37	14	4	1.05	65	65
	max	14	–3.1	910	839	68	43	6	1.08	69	69
27 Mar	median	8.3	–7.2	568	547	39	18	4	1.04	66	63
	min	6.7	–10.4	440	416	32	10	3	1.06	65	60
	max	13.3	–3.0	858	792	71	40	7	1.08	73	72
29 Mar	median	7.7	–7.9	514	499	43	13	5	1.03	67	65
	min	6.6	–10.0	455	444	30	9	3	1.02	64	58
	max	11.7	–3.2	744	684	71	36	6	1.09	69	67
30 Mar	median	7.3	–7.0	531	509	47	12	4	1.04	67	64
	min	5.9	–10.9	403	394	20	6	2	1.02	64	58
	max	11.5	–2.5	741	664	91	45	8	1.12	73	72
31 Mar	median	7.4	–6.6	487	465	35	17	3	1.05	66	63
	min	6.5	–7.3	443	420	32	14	3	1.05	65	60
	max	9.1	–2.5	595	569	63	25	5	1.05	70	67
1 Apr	median	7.1	–6.0	468	449	40	14	4	1.04	66	62
	min	6.3	–9.2	438	421	29	11	3	1.04	55	53
	max	10.4	–3.8	647	597	56	29	5	1.08	70	67
2 Apr	median	7.4	–6.0	492	468	38	16	4	1.05	68	65
	min	6.3	–8.5	430	410	23	13	2	1.05	62	56
	max	10.3	–3.2	662	636	73	35	6	1.04	71	68

consistency study showed these were the most suitable constants for cold waters (Chierici and Fransson, 2009). The calculations were performed on the total hydrogen ion scale (pH_T) using the HSO_4^- dissociation constant of Dickson (1990). In order to investigate the error and variability introduced by using pH measured in melted bulk sea ice, we performed an internal consistency exercise using a comparison between the calculated C_T (C_{Tcalc}) from measured A_T and pH_{15} and the measured C_T (C_{Tmeas}). The data were obtained from analyses of melted ice, sampled in Kongsfjorden in April 2013. The CO_2 system consistency check was performed using four different sets of equilibrium constants of K1 and K2: (1) Roy and others (1993, 1994; hereafter referred to as Roy); (2) Mehrbach and others (1973) refit by Dickson and Millero (1987) (hereafter referred to as Mehr); (3) Millero (1979; hereafter referred to as Millero); and (4) on the GEOSECS NBS scale (from Mehrbach and others, 1973; hereafter referred to as NBS). Figure 3 shows a box-and-whisker plot with the resulting difference between C_{Tmeas} and the calculated C_T based on the four sets of constants ($C_{Tmeas} - C_{Tcalc}$). We found that the C_T values based on the Roy and Mehr constants showed the lowest median deviation from the measured C_T of ~2.7 µmol kg^{-1} (Table 4). They also had the lowest standard error (SE) between the measured and calculated values and the best coefficient of determination (R2). K1 and K2 determined by Millero at zero salinity had the largest median deviation from measured C_T of ~6.3 µmol kg^{-1} (Table 4). In addition, the results from the NBS scale showed a larger median deviation from the measured than the constants estimated based on the sea-water salinity range. This means that by using the Roy constants, the median deviation in the calculated C_T was ~3 µmol kg^{-1} and the SE was ±11 µmol kg^{-1} (Table 4). This standard error of the calculated C_T was considered insignificant in relation to the natural variability in sea ice.

Dissolved inorganic nutrients

Dissolved inorganic nutrients of nitrate ($[NO_3^-]$), phosphate ($[PO_4^{3-}]$) and silicic acid ($[Si(OH)_4]$) were measured on the melted samples, brine, frost-flower melt and UIW. Acid-washed plastic vials were used for sampling. Samples were filtered (0.45 µm) and frozen at –20°C for post-analysis at the Swedish Meteorological and Hydrological Institute, Gothenburg. The nutrients were determined by colorimetric detection and analysed on an auto-analyser using the standard method described by Grasshoff and others (2009).

Microbiological analysis

In general, all ice processing for microbiological analysis was performed at 0°C. Bacterial carbon production (BCP) was measured in centrifuged brine from bulk ice (and in

https://doi.org/10.3189/2015AoG69A563 Published online by Cambridge University Press

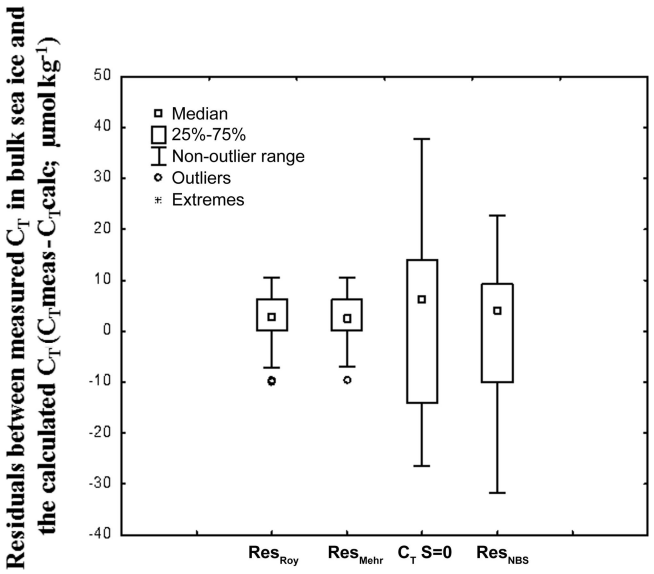

Fig. 3. The residual (µatm) between the measured C_T (C_{Tmeas}) in bulk sea ice and the calculated C_T (C_{Tcalc}) from the four sets of constants: Roy denotes the constants by Roy and others (1993); Mehr denotes the constants by Mehrbach and others (1973), refit by Dickson and Millero (1987); C_T S=0 denotes the constants by Millero (1979) at zero salinity (S = 0); and NBS denotes the constants by the GEOSECS NBS scale from Mehrbach and others (1973). The 25th and 75th percentiles show the limits where 25% and 75% of the residuals fall below. The non-outlier range is the range of values that fall below the upper outer limit of ±1.5× the height of the box (H).

sackholes). Bacterial production (BP) in the drained brine was determined by (^{3}H)-leucine incorporation (Smith and Azam, 1992). The detection limit was 0.5 µg C L^{-1} d^{-1} in the samples. Details on the separation of brine and the methodology for microbiological analysis are thoroughly described by Granfors and others (2013). Sea-ice algae activity and photosynthetic efficiency in the brine were investigated from the maximum quantum yield of photosynthesis (F_v/F_m) using a WATER-PAM chlorophyll fluorometer (Walz Mess- und Regeltechnik, Effeltrich, Germany) and a pulse-amplitude modulated (PAM) fluorometry, respectively. The remaining brine sample was fixed with glutaraldehyde (final concentration 0.1% and 2.5%, respectively) to determine bacterial and microalgal abundance. Samples for bacterial abundance were stored at –80°C for 6 months until analysis, described in Granfors and others (2013).

Table 4. Summary of the resulting median, values at the 25th and 75th percentiles, the standard error (SE) and the coefficient of determination from the regression analysis (R2) of the residual (µatm) between the measured C_T ($C_T$meas) in bulk sea ice and the calculated C_T ($C_T$calc) from each of the four sets of constants: Roy denotes the constants by Roy and others (1993); Mehr denotes Mehrbach and others (1973), refit by Dickson and Millero (1987); at zero salinity (C_T S = 0) from Millero (1979); and on the GEOSECS NBS (NBS) scale from Mehrbach and others (1973). The 25th and 75th percentiles show the limits where 25% and 75% of the residuals fall below

$C_T$meas – $C_T$calc (residuals)	Median	25%	75%	SE	R2
	µmol kg^{-1}			µmol kg^{-1}	
Roy	2.7	0.05	6.3	±10.5	0.955
Mehr	2.6	0.07	6.2	±10.5	0.955
C_T S = 0	6.3	–14	13.9	±20.5	0.883
NBS	4.1	–10	9.2	±17.7	0.892

Table 3. Physical and CO_2-system properties in pancake ice (PCI), landfast sea ice in Engelskbukta (EB, thicker ice), brine (Brine), frost flowers (FF_{new}, FF_{old}), and under-ice water under young ice in Thiisbukta (UIW) and at Engelskbukta (EB). N denotes number of samples and n.a. stands for not applicable

		S	Ice T	A_T	C_T	fCO_2	$[CO_3^{2-}]$	$[CO_2]$	A_T : C_T	A_T : S	C_T : S
			°C	µmol kg^{-1}	µmol kg^{-1}	µatm	µmol kg^{-1}	µmol kg^{-1}			
PCI	median	18.9	–2.5	1227	1156	126	47	10	1.06	65	61
27 Mar	min	16.2	n.a	1055	997	108	40	8	1.06	65	62
30 Mar	max	19.6	n.a	1283	1214	142	51	11	1.06	65	62
EB	median	8.9	–7.6	572	546	406	482	42	1.05	65	61
28 Mar	min	6.3	–10.9	426	409	173	139	20	1.02	63	65
	max	12.5	–3.3	792	703	749	1369	76	1.13	67.5	56
Brine	median	121	–8.4	7481	8019	10 561	114	563	0.93	67	66
	min	119	–9.4	7144	6984	2983	45	166	1.0	67	58
N = 4	max	137	–8.0	8186	9054	18 139	183	959	0.90	68	66
FF_{new}	median	51.6	–15.9	3421	3005	107	274	12.3	1.14	66.4	58
N = 2	min	50.7	–15.9	3386	2990	103	262	11.8	1.13	66.0	59
	max	52.4	–15.9	3456	3020	110	286	12.7	1.14	66.8	58
FF_{old}		53	–14.1	3477	2921	82	364	9	1.14	66.0	55
UIW	median	34.6	–2.0	2289	2147	292.5	103	20	1.07	66.3	62
N = 12	min	34.0		2259	2123	235.3	85	16	1.06	64.2	62
	max	37.0		2375	2219	309.7	121	21	1.08	66.5	60
UIW	median	37.3	–2.0	2403	2249	311	114	21	1.07	64.4	69
EB	min	37.0		2347	2179	269	107	18	1.06	63.4	59
N = 2	max	37.6		2460	2319	353	120	24	1.08	65.4	62

Note: The estimates for A_T and the derived parameters in old brine are based on one value due to the limited sample volume. There are three more data points for salinity, temperature and pH at 15°C.

https://doi.org/10.3189/2015AoG69A563 Published online by Cambridge University Press

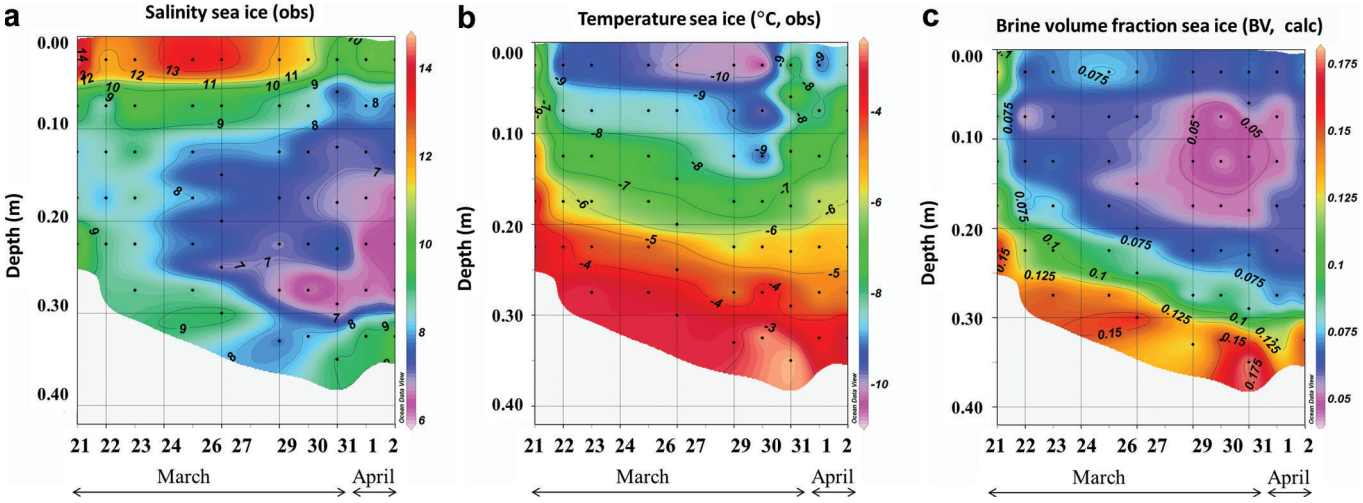

Fig. 4. Vertical and daily distribution of (a) bulk sea-ice salinity, (b) temperature (T; °C) and (c) brine volume fraction (BV) in young landfast sea ice, from 21 March to 2 April 2010; obs and calc denote observed and calculated values, respectively.

Salinity

Salinity and conductivity of the melted sea ice, brine, frost flowers and UIW were measured using a conductivity meter (WTW Cond 330i, Germany) with a resolution and accuracy of ±0.05.

We calculated brine volume fractions (BV) from young-ice salinity (S) and ice temperature (T; °C), according to Frankenstein and Garner (1967) derived from Assur (1958):

$$\mathrm{BV} = \frac{S}{1000}\left(\frac{49.185}{\mathrm{ABS}(T)} + 0.532\right) \quad (2)$$

The ice becomes less permeable as BV decreases (e.g. Golden and others, 2007; Loose and others, 2009, 2010) and both gas and liquid transport decrease. Ice temperature fundamentally controls the ice porosity (Petrich and Eicken, 2010).

Solar radiation

For radiation measurements, a PMA2100 radiometer equipped with a 2π PMA2132 sensor (Solar Light, Philadelphia, PA, USA) was used to record photosynthetic photon flux (PPF) at 400–700 nm (corresponding to photosynthetic active radiation (PAR)) on the pier at Ny-Ålesund, i.e. 500 m from the study site. In addition, PPF was measured in ice with a spherical sensor (QSL-2100, internal diameter 1.25 cm, Biospherical Instruments Inc., San Diego, CA, USA). To avoid shading from the instrument, the sensor was deployed at a 45° angle through the ice.

RESULTS

Physical properties in young sea ice, brine and underlying water

The vertical distribution of salinity in the young-ice cores showed a C-shaped pattern, with higher salinity in the top and bottom ice than in the middle parts, which is typical for first-year ice (e.g. Malmgren, 1927; Thomas and others, 2010), ranging between 14 (22 March) and 10 (31 March) in the top 0.05 m (ice/air interface; Fig. 4a) in young ice. In the interior young ice, the salinity decreased from 9 to 6, whereas in the bottom ice (ice/water interface) little change was observed during the 13 day study. The sea-ice temperature increased linearly with depth from top to bottom and was lowest (–10.9°C) in the top ice, in contact with cold air (Fig. 4b), increasing towards the bottom ice, to reach temperatures close to sea-water temperatures (Fig. 4b; Tables 2 and 3). The coldest ice was observed between 27 and 30 March, when we also recorded the lowest air temperatures.

The thickness of the young ice varied between 0.27 and 0.41 m, with an increase of ~0.011 m d^{-1} (0.14 m increase during the 13 day study) (Table 1). Freeboard was positive throughout the study, suggesting no flooding of the ice, and there was no superimposed ice from melt and refreeze.

BV in the young ice was mostly >0.05, except between 28 March and 1 April, coinciding with the lowest young ice temperatures at depths of 0.05–0.2 m (Fig. 4b and c). These low BV indicated that the mobility of chemical substances (and gases) dissolved in brine was less in the interior ice (BV < 0.05; Cox and Weeks, 1983; Loose and others, 2009, 2010) than in the top and bottom ice (BV > 0.05).

As the thin pancake ice (<0.04 m) formed, ~45% of the ice salinity was lost (from 34 down to 19), showing a substantial and rapid salinity rejection during the formation (Table 3).

Chemical properties in young sea ice, brine and underlying water

All concentrations for bulk sea ice and frost flowers shown in this and following subsections refer to values in melted samples. Young ice (YI) refers to thinner ice from TB, and EB ice refers to thicker ice from Engelskbukta.

CO_2-system evolution

Large variability was observed in all CO_2 system parameters (Fig. 5; Tables 2 and 3). The A_T and C_T of melted samples of young ice (Fig. 5a and b) showed a C-shaped trend each day, similar to salinity, indicating that most of the changes in young-ice C_T and A_T were due to salinity changes. A_T was highest at the ice/air interface compared to the rest of the ice during the 13 day study. The highest value was measured on 22 March, and A_T decreased towards the end of the period (Fig. 5b). Between 24 and 26 March, A_T increased by 120 µmol kg^{-1}, from 790 to 910 µmol kg^{-1}. The calculated concentration of CO_2 ($[CO_2]$) in melted ice was generally lower in the top ice and higher in the bottom ice,

https://doi.org/10.3189/2015AoG69A563 Published online by Cambridge University Press

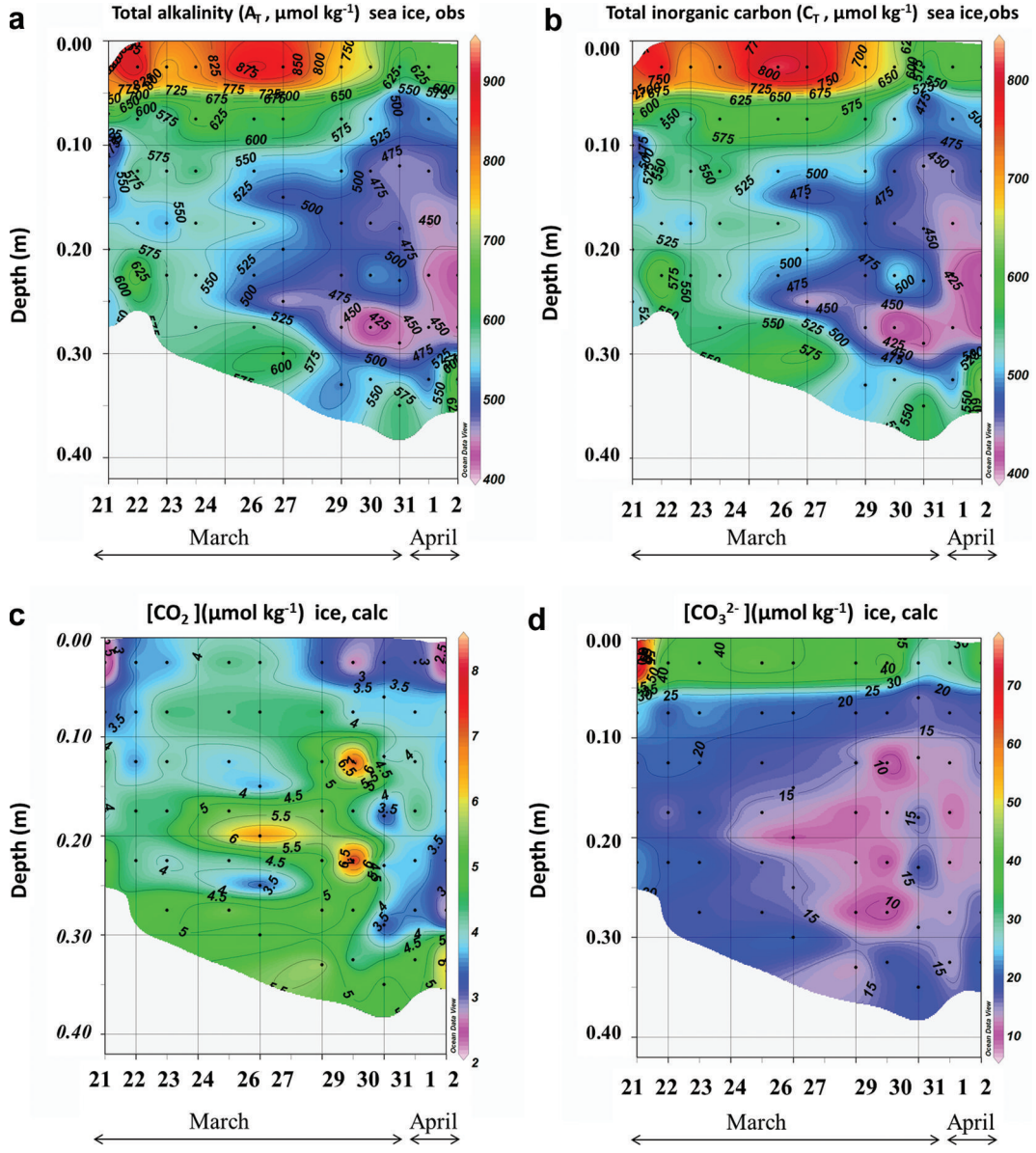

Fig. 5. Vertical and daily distribution of the properties in melted ice of (a) total alkalinity (A_T; µmol kg^{-1}), (b) total inorganic carbon (C_T; µmol kg^{-1}), (c) carbon dioxide concentration ([CO_2]; µmol kg^{-1}) and (d) carbonate ion concentration ([CO_3^{2-}]; µmol kg^{-1}), in young landfast sea ice from 21 March to 2 April 2010; obs and calc denote observed and calculated values in melted sea ice, respectively.

but varied locally on a few occasions (Fig. 5c). [CO_3^{2-}] was highest in the top 0.05 m of the ice and decreased towards the bottom ice (Fig. 5d). In the interior ice, higher [CO_2] land lower [CO_3^{2-}] were found between 27 and 30 March (Fig. 5c and d).

The values of C_T and A_T in melted EB ice were similar to those in melted young ice, but [CO_3^{2-}] and [CO_2] were almost 200 and 10 times larger, respectively, than in young ice (Table 2). The values of C_T, A_T and salinity in melted pancake ice (PCI; newly formed thin ice <0.04 m) were twice as high (Table 3) as in young ice and EB ice. [CO_3^{2-}] and [CO_2] were slightly higher in pancake ice than in young ice, but lower than in EB ice (Table 2). Pancake ice (thin ice) had higher A_T, C_T and salinity than any of the other melted sea-ice samples in the study (Table 3).

Brine concentrations provide an integrated signal of changes in salinity and chemical substances that occurred over time. In our brine samples, [CO_2] was >300 times higher than in melted young ice, whereas [CO_3^{2-}] in brine was of the same order of magnitude as in melted young ice (Tables 2 and 3). The fugacity of CO_2 (fCO_2) values in our brine samples was up to 18 000 µatm (1824 Pa) (Table 3).

The salinity, A_T and C_T values of UIW at the EB site were, on average, higher than the UIW values in TB.

Nutrients evolution

In young ice, [NO_3^-] and [$Si(OH)_4$] did not change significantly during the study, but [PO_4^{3-}] decreased from 0.2 to 0.04 mmol m^{-3} in melted ice during the growth of the young ice (Table 5). The nutrient concentrations in the EB ice were, on average, similar to those in the young ice at the end of the study (Table 5). In brine, the nutrient concentrations were higher than in the melted young ice, with [PO_4^{3-}] 10 times higher and [NO_3^-] and [$Si(OH)_4$] ~15 times higher (Table 5). In UIW, the concentrations of all three measured nutrients decreased during the study, with [PO_4^{3-}] decreasing from 1.1 to 0.66, [NO_3^-] from 14.7 to 8.5 and [$Si(OH)_4$] from 7.0 to 3.9 µM.

https://doi.org/10.3189/2015AoG69A563 Published online by Cambridge University Press

Table 5. Inorganic nutrients (phosphate (PO_4^{2-}), nitrate (NO_3^-), silicic acid ($Si(OH)_4$) in young landfast sea ice (YI), landfast sea ice from Engelskbukta (EB), brine, and frost flower (FF). * denotes that brine values are mean values from four sampling occasions. Minimum and maximum values are denoted min and max, respectively

Type	Date (2010)		PO_4^{2-}	NO_3^-	$Si(OH)_4$
			mmol m^{-3}	mmol m^{-3}	mmol m^{-3}
YI	23 Mar	median	0.20	2.00	1.04
		min	0.14	1.94	0.98
		max	0.46	7.33	3.13
YI	24 Mar	median	0.16	2.40	1.16
		min	0.03	2.12	1.08
		max	0.22	3.22	1.28
YI	29 Mar	median	0.04	1.78	0.92
		min	0.02	1.47	0.77
		max	0.09	4.10	1.35
EB	28 Mar	median	0.07	1.90	0.96
		min	0.02	1.20	0.72
		max	0.14	3.70	1.36
Brine (EB)	28 Mar	$N = 1$	1.9	23	11
Brine (YI)	$N = 4$*	mean/stdev	2.0 ± 0.04	33 ± 2	15 ± 1
FF new	27 Mar	mean/stdev	1.0 ± 0.1	14 ± 1	7 ± 0.1

Biological properties in sea-ice brines, frost flowers and underlying water

Abundance and activity of heterotrophic bacteria

In all the ice samples, there was a standing stock of heterotrophic bacteria in young ice with bacteria present. The BCP ranged between 0.5 and 9.1 μg C L^{-1} d^{-1} during the study. The highest value of BCP (9.1 μg C L^{-1} d^{-1}) was detected on 29 March in the interior of young ice, corresponding to an increase of inorganic carbon by 0.8 μmol C kg^{-1} d^{-1}. In the brine from centrifuged bulk ice, the bacterial abundance varied between 7.1×10^7 and 6.4×10^8 cells L^{-1}. This was of the same order of magnitude as other measurements made in winter Arctic sea ice (Junge and others, 2004) of 10^7–10^9 cells L^{-1}.

In the EB ice, the BCP was higher (up to 14 μg C L^{-1} d^{-1}) than in young ice, with higher values in the top ice and bottom ice. In the frost flowers, the BCP was 2.8 μg C L^{-1} d^{-1}. The BCP in UIW was 1.3 μg C L^{-1} d^{-1} on 23 March, with a maximum value of ~5.0 μg C L^{-1} d^{-1} on 24 March. It was 1.4 μg C L^{-1} d^{-1} on 26 March, and decreased towards the end of the study.

Abundance and activity of microalgae

Microalgae were quantifiable in the bottom layer of the young-ice core. The abundances varied between 7.1×10^4 and 8.8×10^5 cells L^{-1} in centrifuged brine. The most frequently occurring microalgal genera were pennate diatoms *Synedropsis* sp., and *Fragilariopsis* sp., which is typical for ice algal communities. During the study, we measured photosynthetically active algal cells in the young ice. Our estimates of F_v/F_m varied between 0.06 and 0.5. The maximum quantum yield of photosynthesis (F_v/F_m, a measure of the health of the algae) could be measured in the bottom 0.05 m (ice/water interface) of the young ice. The F_v/F_m was 0.06 at the start on 23 March (bottom 0.05 m) and increased to a maximum of 0.5 on 26 March, likely due to the maximum solar radiation on 26 March.

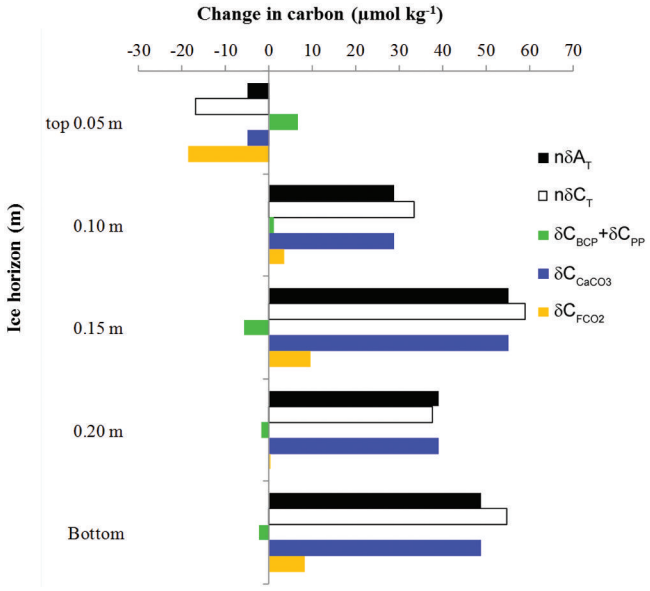

Fig. 6. The change (μmol kg^{-1}) at five different ice horizons in the young ice from top to bottom in salinity-normalized total alkalinity ($n\delta A_T$, black) and total inorganic carbon ($n\delta C_T$, white). The change in nC_T due to processes other than salinity changes is the combined effect of the biological processes of primary production and bacterial-carbon production ($\delta C_{PP} + \delta C_{BCP}$, green) estimated from salinity-normalized [NO_3^-] change, the effect of calcium carbonate precipitation and dissolution (δC_{CaCO3}, blue) based on $n\delta A_T$, and CO_2-gas flux (δC_{FCO2}, orange). The change was estimated from the start (21 March 2010, day 1) to the end of the study period (2 April 2010, day 13). Positive change denotes a gain in carbon, and negative change a loss of carbon from the ice horizon.

There were fewer ice algal cells and lower F_v/F_m (0.07–0.25) in the EB bottom ice than the TB young ice. Moreover, the ice algae in the EB thick ice were distributed in the bottom 0.10 m of ice instead of being restricted to the bottom 0.05 m.

Processes driving the CO_2 system

To eliminate the effect of salinity on the changes in young-ice C_T and A_T, we used the mean young-ice salinity (S_{ice}) of 8.8 (following a dilution line; $nC = 8.8/S_{ice}C$, where C represents young-ice C_T, A_T and nitrate) to obtain salinity-normalized values, hereafter referred to as $n\delta C_T$ and $n\delta A_T$. The $n\delta C_T$ and $n\delta A_T$ values showed a net increase at all ice horizons except in the top 0.05 m of the ice, where both parameters showed a net decrease over the whole study period (Fig. 6). This estimate was based on the difference between the values on 21 March and 2 April (Fig. 6). The main processes driving the changes in $n\delta C_T$ are biological processes such as primary production (δC_{PP}), bacterial carbon production (δC_{BCP}), $CaCO_3$ precipitation and dissolution (δC_{CaCO3}) and CO_2 gas flux (δC_{FCO2}),

$$n\delta CT = \delta C_{BCP} + \delta C_{PP} + \delta C_{CaCO3} + \delta C_{FCO2} \quad (3)$$

while $n\delta A_T$ is mainly affected by $CaCO_3$ precipitation and dissolution.

To calculate the net effect of biological processes, we used the change in salinity-normalized nitrate concentrations ($n\delta[NO_3^-]$) converted to carbon equivalents using the stoichiometric carbon and nitrogen ratios of 106 : 16 after

https://doi.org/10.3189/2015AoG69A563 Published online by Cambridge University Press

Redfield and others (1963). We found significant changes in $n\delta[NO_3^-]$ in the top 0.05 m and in the top 0.15 m young-ice horizons during the study period. In the interior ice (at 0.15 m), we found a net $n\delta[NO_3^-]$ decrease of 0.9 mmol m^{-3}, corresponding to a carbon uptake of 6 μmol kg^{-1} due to primary production (δC_{PP}; Fig. 6). The fact that we observed photosynthetic activity with significant algae abundances (7×10^4 and 8.8×10^5 cells mL^{-1}) implies that such organisms were partly responsible for the variations found in $n\delta[NO_3^-]$ and young ice $[CO_2]$ after 25 March (Fig. 5c). The yield was highest in the bottom ice. At the same time as we found a net carbon uptake, we also found the highest measured BCP of 9.1 μg C L^{-1} d^{-1} in the interior of the ice (maximum on 29 March 2010), corresponding to an increase in inorganic carbon of 0.8 μmol L^{-1} d^{-1}. Denitrification by bacteria could also explain the $n[NO_3^-]$ decrease (Rysgaard and Glud, 2004). In the top 0.05 m we found a small but significant net increase in $n\delta[NO_3^-]$ of 1 mmol m^{-3}, corresponding to a C_T increase of 7 μmol kg^{-1}, likely due to BCP (δC_{BCP}; Fig. 6).

The sum of the effects of $CaCO_3$ formation and dissolution and CO_2 gas flux was obtained by calculating the difference between $n\delta C_T$ and the values from biological processes:

$$\delta C_{CaCO3} + \delta C_{FCO2} = n\delta CT - \delta C_{BCP} - \delta C_{PP} \quad (4)$$

Based on the correction of $n\delta C_T$ due to biological processes ($n\delta C$bio), there was nonetheless a net C_T loss at the top 0.05 m ice horizon and a larger gain at the 0.15 m ice horizon and at all other horizons (Fig. 6). A similar pattern was found for $n\delta A_T$ (Fig. 6). Between the interior ice and the basal ice, $n\delta A_T$ increased by 40–55 μmol kg^{-1}, mostly explained by the effect of $CaCO_3$. We estimated the net CO_2 gas flux

$$\delta C_{FCO2} = +n\delta CT - \delta C_{BCP} - \delta C_{PP} - \delta C_{CaCO3} \quad (5)$$

resulting in a negative CO_2 gas flux (loss of 20 μmol kg^{-1} melted ice) at the top 0.05 m ice horizon and a positive CO_2 gas flux (gain of maximum 10 μmol kg^{-1}) in the interior ice and in the bottom ice (Fig. 6). The CO_2 loss from the 0.05 m of top ice to the atmosphere was estimated as ~1 mmol m^{-2} (or 12 mg C m^{-2}) or 0.08 mmol m^{-2} d^{-1} melted ice.

Frost flowers and ice–air CO_2 gas flux

On 26 March the weather conditions were cold with little wind (wind speed of 0.9 m s^{-1}) and an air temperature of –15.6°C. The relative humidity was the highest during the study (73%; Table 1). New thin sea ice and new frost flowers were formed further out in the bay, 200 m from our study site. Elevated concentrations of A_T (3421 μmol kg^{-1}) and C_T (3005 μmol kg^{-1}) were observed in the new frost-flower melt, which were substantially higher than the UIW concentrations but less than in the brine (Table 3). The lower C_T in frost-flower melt compared to brine C_T means that there was a loss of C_T (i.e. CO_2) probably before our first sampling. When the frost flowers from the same location were sampled 20 hours later, ~25% (from 12 to 9 μmol kg^{-1}) of the CO_2 content in the frost-flower melt had disappeared. The salinity in the frost flowers had changed by 1 after 20 hours, supporting the fact that processes other than salinity changes were affecting the CO_2 concentrations and C_T (e.g. air–ice CO_2 flux). Similar to salinity, A_T did not change significantly, but $[CO_3^{2-}]$ in the melted frost flowers increased (Table 3), which suggests influence of CO_2 loss. Additionally, C_T in the frost-flower melt decreased from 3005 μmol kg^{-1} to 2921 μmol kg^{-1}, resulting in a C_T loss of 84 μmol kg^{-1} d^{-1}, likely due to CO_2 loss to the atmosphere (Table 3). The BCP was 2.8 μg C L^{-1} d^{-1} (i.e. 0.23 μmol kg^{-1} d^{-1}) in the 1 day old frost-flower melt, which was insignificant relative to the uncertainty in the C_T analysis. Using salinity-normalized ($S = 52$) C_T for both days during the frost-flower melt, the resulting CO_2 loss was 142 μmol kg^{-1} d^{-1} (7 mmol m^{-2} d^{-1}). After frost-flower formation, the life span of the frost flowers at the sampling site was ~48 hours.

When $[CO_2]$ in brine was high, the CO_2 loss through frost flowers could have an impact on the atmospheric CO_2 concentrations (mainly near the ice surface). Since CO_2 easily escapes from the ice when the ice is porous enough (BV > 0.05), the frost flowers form an efficient transport path for CO_2 from the ice to the atmosphere (e.g. Fransson and others, 2013; Geilfus and others, 2013). We used the formulation by Fransson and others (2013) to estimate the C_T loss and CO_2 outflow from sea ice to atmosphere through frost flowers and brine of Arctic sea ice:

$$C_{Tcalc} = S_{FF}/S_{brine} \cdot C_{Tbrine} \quad (6)$$

$$C_{Tout} = C_{Tcalc} - C_{TFF} \quad (7)$$

where S_{FF} and S_{brine} are the salinity of frost-flower melt (average $S = 51$) and brine ($S = 121$), respectively. C_{TFF} and C_{Tbrine} are the C_T in frost-flower melt ($C_T = 3000$ μmol kg^{-1}) and brine ($C_T = 9054$ μmol kg^{-1}). This gives a C_{Tcalc} of 3816 μmol kg^{-1}), resulting in a maximum CO_2 loss (C_{Tout}) of 816 μmol kg^{-1} d^{-1} (~40 mmol m^{-2} d^{-1}) from the ice to the atmosphere, assuming no biological production. The salinity-normalized ($S = 121$) nutrient ($[PO_4^{3-}]$, $[NO_3^-]$, $[Si(OH)_4]$) concentrations in new frost flowers were the same as those in brine (Table 5), which supports our assumption that, in our study, no CO_2 was consumed associated with primary production. Moreover, since the fCO_2 values in both brine and frost-flower melt (Tables 2 and 3) were much larger than the atmospheric fCO_2 value of ~394 μatm (39.9 Pa; Ny-Ålesund 2010), frost flowers show a great potential to act as a CO_2 source to the atmosphere.

DISCUSSION

We found that the C_T loss from frost flowers was due to a CO_2 loss of 40 mmol m^{-2} d^{-1} melted sample mediated by upward-transported brine and by frost-flower formation. Our estimates were similar to the findings by Geilfus and others (2013), which estimated a CO_2 loss from the ice to the atmosphere of 20–40 mmol m^{-2} d^{-1} melted sample. These estimates indicate the efficient transfer of CO_2 by frost flowers and a large potential for CO_2 loss during a short period. Moreover, the mean calculated fCO_2 in brine was 10 560 μatm (1070 Pa), which was several times higher than the atmospheric values of ~400 μatm (40.5 Pa), supporting a large potential for a CO_2 loss from the ice due to ice dynamics. Using our estimates of CO_2 loss by the frost flowers of 0.8 mol m^{-3} melted sample (800 mmol m^{-3}) and assuming that the frost flowers formed at least on one day (24 hour life cycle) on top of all newly formed spring ice in the Arctic Ocean (area of 14×10^6 km^{-2} (US National Snow and Ice Data Center, mean sea-ice covered area in April 2010)), we obtain a total CO_2 gas flux to the atmosphere of 0.2×10^{13} to 1.1×10^{13} mol C (0.02–0.13 Pg C) in one day. This estimate can be compared to the summer net CO_2 uptake of 0.1 Pg C a^{-1} in the Arctic Ocean based on Schuster and others (2013). However, although it is likely that this is an overestimation, it strongly supports the fact that frost flowers play a large role in the CO_2 outgassing from the sea

https://doi.org/10.3189/2015AoG69A563 Published online by Cambridge University Press

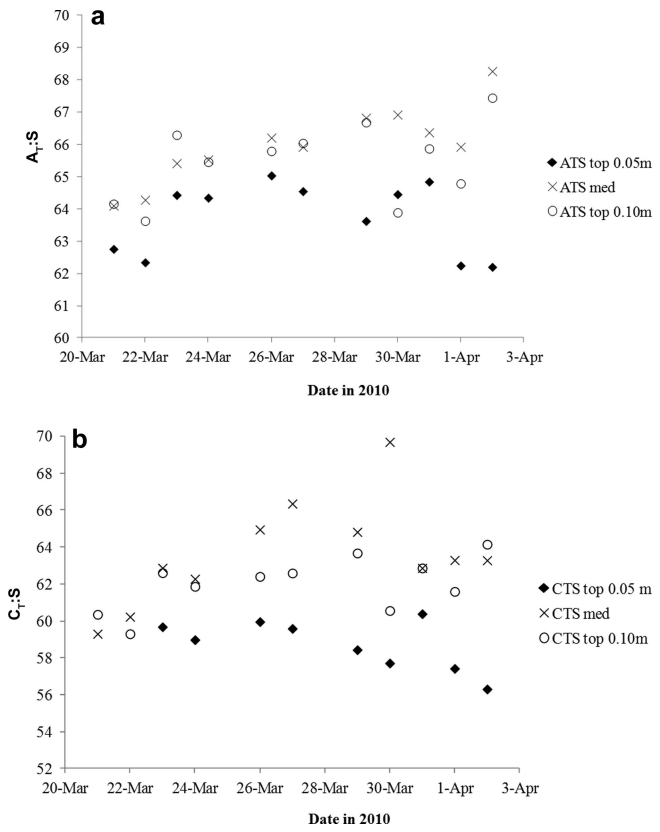

Fig. 7. The variability of (a) the A_T:salinity ratio ($A_T : S$) and (b) the C_T:salinity ratio ($C_T : S$) in the top 0.05 m (filled diamonds), top 0.10 m (open circles) and median sea ice (crosses) for the whole study.

water, and that the role of frost flowers in CO_2 air–ice flux needs further investigation.

To further investigate the variability of nA_T (and nC_T) in the young ice, we used the ratios between A_T and salinity ($A_T : S$) as proxies for $CaCO_3$ precipitation in sea ice (e.g. Fransson and others, 2011, 2013; Rysgaard and others, 2012). Increasing $A_T : S$ means fractionation of A_T and salinity, likely indicating the presence and dissolution of solid $CaCO_3$. Except for in the top 0.05 m, the $A_T : S$ ratio in melted young ice increased (Table 2). Based on the $A_T : S$-ratio development during the study (Fig. 7a), we distinguished a pattern in the variability of the ice horizons, which may be due to changes in A_T relative to salinity or transport of $CaCO_3$ to underlying ice horizons during ice formation (Fig. 7a). Moreover, we found that the $A_T : S$ variability in the top 0.05 m ice corresponded to changes in air temperature. The lowest air temperature was recorded on 27, 29 and 30 March, shifting to warmer air on 30–31 March (Table 1). The increased air and young-ice temperatures caused an increase in BV, allowing chemical substances to move through the ice in brine channels.

CONCLUSION

In this wintertime study of growing young ice, we found changes in the sea-ice CO_2 system at all ice horizons. At the ice/air interface (top 0.05 m), we found that nC_T decreased in the ice due to CO_2 loss to the atmosphere during our study and that nC_T and nA_T increased at underlying horizons. The ice–air CO_2 gas flux was partly driven by the process of $CaCO_3$ precipitation within the ice, as was also concluded by Geilfus and others (2013). The amount of solid $CaCO_3$ estimated for the 13 day study was smaller or in the same order of magnitude as found by Fransson and others (2013) and Rysgaard and others (2013). Biological processes were active only to a limited extent in the young ice during the study but imposed local effects on the sea-ice CO_2 system.

Our study confirms previous results that frost flowers are important conveyors for CO_2 gas exchange from ice to atmosphere during ice formation. Assuming that frost flowers will form on newly formed sea ice, this source of CO_2 to the atmosphere would be similar to the net CO_2 uptake in the Arctic Ocean (Schuster and others, 2013). Our study implies that CO_2 loss from frost flowers may be more important for the air–ice–sea CO_2 transfer for the Arctic Ocean than previously reported.

ACKNOWLEDGEMENTS

This is a contribution to the project 'Greenhouse gases and mercury in a changing Arctic', funded by the Swedish Research Council (No. 2007-8365). We thank the Norwegian Meteorological Institute for making their meteorological and ice concentration data available (www.met.no). We thank the personnel at the Sverdrup station (Norwegian Polar Institute) in Ny-Ålesund for logistic support. We also thank two anonymous reviewers for constructive comments, which improved the manuscript.

REFERENCES

Alvarez-Aviles L, Simpson WR, Douglas TA, Sturm M, Perovich D and Domine F (2008) Frost flower chemical composition during growth and its implications for aerosol production and bromine activation. *J. Geophys. Res.*, **113**(D21), D21304 (doi: 10.1029/2008JD010277)

Assur A (1958) Composition of sea ice and its tensile strength. In *Arctic Sea Ice. Proceedings of the Conference held 24–27 February 1958, Easton, MD, USA*. (National Research Council Publication 598) US National Academy of Sciences, Washington, DC, 106–138

Chierici M and Fransson A (2009) Calcium carbonate saturation in the surface water of the Arctic Ocean: undersaturation in freshwater influenced shelves. *Biogeosciences*, **6**(11), 2421–2431 (doi: 10.5194/bg-6-2421-2009)

Chierici M, Fransson A and Anderson LG (1999) Influence of *m*-cresol purple indicator additions on the pH of seawater samples: correction factors evaluated from a chemical speciation model. *Mar. Chem.*, **65**(3–4), 281–290 (doi: 10.1016/S0304-4203(99)00020-1)

Clayton TD and Byrne RH (1993) Spectrophotometric seawater pH measurements: total hydrogen ion concentration scale calibration of *m*-cresol purple and at-sea results. *Deep-Sea Res. I*, **40**(10), 2115–2129 (doi: 10.1016/0967-0637(93)90048-8)

Cox GFN and Weeks WF (1983) Equations for determining the gas and brine volumes in sea-ice samples. *J. Glaciol.*, **29**(102), 306–316

DeLille B, Jourdain B, Borges AV, Tison J-L and DeLille D (2007) Biogas (CO_2, O_2, dimethylsulfide) dynamics in spring Antarctic fast ice. *Limnol. Oceanogr.*, **52**(4), 1367–1379 (doi: 10.4319/lo.2007.52.4.1367)

Deming JW (2010) Sea ice bacteria and viruses. In Thomas DN and Dieckmann GS eds *Sea ice*. Wiley-Blackwell, Chichester, 247–282

Dickson AG (1990) Standard potential of the reaction: AgCl(s) + ½H_2(g) = Ag(s) + HCl(aq), and the standard acidity constant of

https://doi.org/10.3189/2015AoG69A563 Published online by Cambridge University Press

the ion HSO_4^- in synthetic sea water from 273.15 to 318.15 K. *J. Chem. Thermodyn.*, **22**(2), 113–127 (doi: 10.1016/0021-9614(90)90074-Z)

Dickson AG (1993) The measurement of sea water pH. *Mar. Chem.*, **44**(2–4), 131–142 (doi: 10.1016/0304-4203(93)90198-W)

Dickson AG and Millero FJ (1987) A comparison of the equilibrium constants for the dissociation of carbonic acid in seawater media. *Deep-Sea Res. I*, **34**(10), 1733–1743 (doi: 10.1016/0198-0149(87)90021-5)

Dickson AG, Sabine CL and Christian JR eds (2007) *Guide to best practices for ocean CO_2 measurements*. (PICES Special Publication 3) North Pacific Marine Science Organization, Sidney, BC

Dieckmann GS and 6 others (2010) Ikaite ($CaCO_3{\cdot}6H_2O$) discovered in Arctic sea ice. *Cryosphere*, **4**(2), 227–230 (doi: 10.5194/tc-4-227-2010)

Domine F, Taillandier AS, Simpson WR and Severin K (2005) Specific surface area, density and microstructure of frost flowers. *Geophys. Res. Lett.*, **32**(13), L13502 (doi: 10.1029/2005GL023245)

Douglas TA and 11 others (2012) Frost flowers growing in the Arctic ocean–atmosphere–sea ice–snow interface: 1. Chemical composition. *J. Geophys. Res.*, **117**(D14), D00R09 (doi: 10.1029/2011JD016460)

Else BGT, Papakyriakou TN, Galley RJ, Drennan WM, Miller LA and Thomas H (2011) Wintertime CO_2 fluxes in an Arctic polynya using eddy covariance: evidence for enhanced air–sea gas transfer during ice formation. *J. Geophys. Res.*, **116**(C9), C00G03 (doi: 10.1029/2010JC006760)

Else BGT and 7 others (2012) Annual cycles of pCO_{2sw} in the southeastern Beaufort Sea: new understandings of air–sea CO_2 exchange in arctic polynya regions. *J. Geophys. Res.*, **117**(C9), C00G13 (doi: 10.1029/2011JC007346)

Frankenstein G and Garner R (1967) Equations for determining the brine volume of sea ice from –0.5°C to –22.9°C. *J. Glaciol.*, **6**(48), 943–944

Fransson A, Chierici M, Yager PL and Smith WO Jr (2011) Antarctic sea ice carbon dioxide system and controls. *J. Geophys. Res.*, **116**(C12), C12035 (doi: 10.1029/2010JC006844)

Fransson A and 7 others (2013) Impact of sea-ice processes on the carbonate system and ocean acidification at the ice–water interface of the Amundsen Gulf, Arctic Ocean. *J. Geophys. Res.*, **118**(12), 7001–7023 (doi: 10.1002/2013JC009164)

Geilfus N-X and 7 others (2013) First estimates of the contribution of $CaCO_3$ precipitation to the release of CO_2 to the atmosphere during young sea ice growth. *J. Geophys. Res.*, **118**(1), 244–255 (doi: 10.1029/2012JC007980)

Golden KM, Eicken H, Heaton AL, Miner J, Pringle DJ and Zhu J (2007) Thermal evolution of permeability and microstructure in sea ice. *Geophys. Res. Lett.*, **34**(16), L16501 (doi: 10.1029/2007GL030447)

Granfors A and 7 others (2013) Biogenic halocarbons in young Arctic sea ice and frost flowers. *Mar. Chem.*, **155**, 124–134 (doi: 10.1016/j.marchem.2013.06.002)

Grasshoff K, Ehrhardt M and Kremling K eds (2009) *Methods of seawater analysis*, 3rd edn. Wiley VCH, Weinheim

Hare AA, Wang F, Barber D, Geilfus N-X, Galley RJ and Rysgaard S (2013) pH evolution in sea ice grown at an outdoor experimental facility. *Mar. Chem.*, **154**, 46–54 (doi: 10.1016/j.marchem.2013.04.007)

Junge K, Eicken H and Deming JW (2004) Bacterial activity at –2 to –20°C in Arctic wintertime sea ice. *Appl. Environ. Microbiol.*, **70**(1), 550–557 (doi: 10.1128/AEM.70.1.550-557.2004)

Loose B, McGillis WR, Schlosser P, Perovich D and Takahashi T (2009) Effects of freezing, growth, and ice cover on gas transport processes in laboratory seawater experiments. *Geophys. Res. Lett.*, **36**(5), L05603 (doi: 10.1029/2008GL036318)

Loose B and 9 others (2010) Gas diffusion through columnar laboratory sea ice: implications for mixed-layer ventilation of CO_2 in the seasonal ice zone. *Tellus B*, **63**(1), 23–29 (doi: 10.1111/j.1600-0889.2010.00506.x)

Lyakhin YI (1970) Saturation of water of the Sea of Okhotsk with calcium carbonate. *Oceanology*, **10**, 789–795

Malmgren F (1927) On the properties of sea ice. In Sverdrup HU ed. *The Norwegian North Polar Expedition with the 'Maud' 1918–1925: scientific results, Vol. 1*. John Griegs Boktr, Bergen, 1–67

Mehrbach C, Culberson CH, Hawley JE and Pytkowicz RM (1973) Measurement of the apparent dissociation constants of carbonic acid in seawater at atmospheric pressure. *Limnol. Oceanogr.*, **18**(6), 897–907 (doi: 10.4319/lo.1973.18.6.0897)

Miller LA and 9 others (2011a) Carbon dynamics in sea ice: a winter flux time series. *J. Geophys. Res.*, **116**(C2), C02028 (doi: 10.1029/2009JC006058)

Miller LA, Carnat G, Else BGT, Sutherland N and Papakyriakou TN (2011b) Carbonate system evolution at the Arctic Ocean surface during autumn freeze-up. *J. Geophys. Res.*, **116**(C9), C00G04 (doi: 10.1029/2011JC007143)

Millero FJ (1979) The thermodynamics of the carbonate system in seawater. *Geochim. Cosmochim. Acta*, **43**(10), 1651–1661 (doi: 10.1016/0016-7037(79)90184-4)

Nomura D, Yoshikawa-Inoue H and Toyota T (2006) The effect of sea-ice growth on air–sea CO_2 flux in a tank experiment. *Tellus B*, **58**(5), 418–426 (doi: 10.1111/j.1600-0889.2006.00204.x)

Nomura D, Takatsuka T, Ishikawa M, Kawamura T, Shirasawa K and Yoshikawa-Inoue H (2009) Transport of chemical components in sea ice and under-ice water during melting in the seasonally ice-covered Saroma-ko Lagoon, Hokkaido, Japan. *Estuar. Coast. Shelf Sci.*, **81**(2), 201–209 (doi: 10.1016/j.ecss.2008.10.012)

Nomura D and 8 others (2013) Characterization of ikaite ($CaCO_3{\cdot}6H_2O$) crystals in first-year Arctic sea ice north of Svalbard. *Ann. Glaciol.*, **54**(62 Pt 1), 125–131 (doi: 10.3189/2013AoG62A034)

Papadimitriou S, Kennedy H, Kattner G, Dieckmann GS and Thomas DN (2004) Experimental evidence for carbonate precipitation and CO_2 degassing during sea ice formation. *Geochim. Cosmochim. Acta*, **68**(8), 1749–1761 (doi: 10.1016/j.gca.2003.07.004)

Papakyriakou T and Miller L (2011) Springtime CO_2 exchange over seasonal sea ice in the Canadian Arctic Archipelago. *Ann. Glaciol.*, **52**(57 Pt 2), 215–224 (doi: 10.3189/172756411795931534)

Parkinson CL and Comiso JC (2013) On the 2012 record low Arctic sea ice cover: combined impact of preconditioning and an August storm. *Geophys. Res. Lett.*, **40**(7), 1356–1361 (doi: 10.1002/grl.50349)

Perovich DK and Richter-Menge JA (1994) Surface characteristics of lead ice. *J. Geophys. Res.*, **99**(C8), 16 341–16 350 (doi: 10.1029/94JC01194)

Petrich C and Eicken H (2010) Growth, structure and properties of sea ice. In Thomas DN and Dieckmann GS eds *Sea ice*. Wiley-Blackwell, Chichester, 23–77

Pierrot DE, Lewis E and Wallace D. (2006) *MS Excel program developed for CO_2 system calculations. ORNL/CDIAC-105*. Carbon Dioxide Information Analysis Center, Oak Ridge National Laboratory, US Department of Energy, Oak Ridge, TN

Redfield AC, Ketchum BH and Richards FA (1963) The influence of organisms on the composition of seawater. In Hill MN ed. *The sea, Vol. 2*. Wiley Interscience, New York, 26–77

Roy RN and 7 others (1993) The dissociation constants of carbonic acid in seawater at salinities 5 to 45 and temperatures 0 to 45°C. *Mar. Chem.*, **44**(2–4), 249–267 (doi: 10.1016/0304-4203(93)90207-5)

Roy RN and 7 others (1994) Erratum: the dissociation constants of carbonic acid in seawater at salinities 5 to 45 and temperatures 0 to 45°C. *Mar. Chem.*, **45**(4), 337 (doi: 10.1016/0304-4203(94)90077-9)

Rysgaard S and Glud RN (2004) Anaerobic N_2 production in Arctic sea ice. *Limnol. Oceanogr.*, **49**(1), 86–94 (doi: 10.4319/lo.2004.49.1.0086)

Rysgaard S, Glud RN, Sejr MK, Bendtsen J and Christensen PB (2007) Inorganic carbon transport during sea ice growth and

https://doi.org/10.3189/2015AoG69A563 Published online by Cambridge University Press

decay: a carbon pump in polar seas. *J. Geophys. Res.*, **112**(C3), C03016 (doi: 10.1029/2006JC003572)

Rysgaard S and 7 others (2012) Ikaite crystals in melting sea ice: implications for pCO_2 and pH levels in Arctic surface waters. *Cryosphere*, **6**(4), 901–908 (doi: 10.5194/tc-6-901-2012)

Rysgaard S and 14 others (2013) Ikaite crystal distribution in winter sea ice and implications for CO_2 system dynamics. *Cryosphere*, **7**(2), 707–718 (doi: 10.5194/tc-7-707-2013)

Schuster U and 21 others (2013) An assessment of the Atlantic and Arctic sea–air CO_2 fluxes, 1990–2009. *Biogeosciences*, **10**(1), 607–627 (doi: 10.5194/bg-10-607-2013)

Smith DC and Azam F (1992) A simple, economical method for measuring bacterial protein synthesis rates in sea-water using 3H-leucine. *Mar. Microb. Food Webs*, **6**(2), 107–114

Thomas DN, Papadimitriou S and Michel C (2010) Biogeochemistry of sea ice. In Thomas DN and Dieckmann GS eds *Sea ice*. Wiley-Blackwell, Chichester, 425–467

Yao W, Liu X and Byrne RH (2007) Impurities in indicators used for spectrophotometric seawater pH measurements: assessment and remedies. *Mar. Chem.*, **107**(2), 167–172 (doi: 10.1016/j.marchem.2007.06.012)

https://doi.org/10.3189/2015AoG69A563 Published online by Cambridge University Press